



A Very Large Lepton Collider in the VLHC tunnel

Tanaji Sen

FNAL, P.O. Box 500, Batavia, IL 60510

and

Jim Norem

HEP Division, ANL, Argonne, IL 60439

Abstract

The Very Large Hadron Collider (VLHC) design is converging on a program where a 233 km circumference tunnel would first be occupied by a low field dipole system producing 40 TeV in the center of mass, followed by a higher field magnet system producing nearly 200 TeV in the center of mass. We consider the possibility of first using the tunnel for a large e^+e^- collider, which could operate in the range $90 < E_{cm} < 400$ GeV. This device would be a relatively conservative extrapolation of LEP technology. We assume that the total radiated synchrotron power will be limited to 100 MW. We describe the design strategy, the luminosity and energy reach, the factors that limit the machine performance, the scaling laws that apply to its design, and the technology that would be required for its implementation.

Contents

1	Introduction	3
2	Design Strategy	3
2.1	Bunch intensity limitations	4
2.2	Beam intensity limitations	5
2.3	Synchrotron radiation power and beam-beam limited regime	5
2.4	RF parameters	6
2.5	Optics	7
2.5.1	Arc optics	7
2.5.2	Interaction Region	9
2.6	Summary of design strategy	10
3	Lifetime	10
4	Scaling of the beam-beam parameter	11
5	Polarization	11
6	Design Parameters at High Energy	14
7	Operation at 45 GeV	18
8	Scaling Laws with Energy	22
9	An Injector System	23
10	Technological Challenges	24
10.1	Vacuum System	24
10.2	Cooling System	25
10.3	Magnet Design	25
10.4	Other Components	26
11	Conclusions	27
A	Appendix: Useful Symbols and Formulae	30

1 Introduction

Plans for the future very large hadron collider (VLHC) now envisage a staging scenario [1] where a low field collider would be built first followed by a high field collider in the same tunnel several years later. There is also interest in an electron-positron collider in the same tunnel which could study physics that would complement the studies with the hadron collider. This machine could be used to, 1) examine the W and Z^0 with high precision, to improve measurements of electroweak parameters by an order of magnitude, 2) study continuum fermion pair production, 3) produce clean Higgs mesons at an energy of perhaps 115 GeV, 4) measure the W mass from W pair production thresholds, and 5) look at the $t\bar{t}$ thresholds with very good energy resolution [2]. The very large circumference of the tunnel makes it possible to think of an $e^+ - e^-$ ring which could reach an energy about twice that of LEP if we limit the synchrotron radiation power to 100 MW. Compared to the NLC, the energy and luminosity reach of such a machine is lower. However the technology required is proven and available today. We believe that such a large lepton collider can be built with conservative assumptions and at a fraction of the current estimated cost of the NLC. In this paper we outline the design of this collider and consider some of the accelerator physics issues. We compare and contrast the parameters of this machine with LEP. Much of the material on LEP is obtained from a recent workshop on the subject of “ e^+e^- in the VLHC” [3], and a recent paper by Brandt et al. [4]. We attempt to identify the mechanisms that will limit the performance of the collider and look at scaling laws for the operation of such a machine at high energies. We also attempt to identify methods that could perhaps be used to both increase the performance of the machine and reduce the cost of the facility.

2 Design Strategy

Our design philosophy of this electron-positron collider will be to avail of the maximum RF power available and operate at the beam-beam limit. The synchrotron radiation power lost by *both beams*, each with beam current I is

$$P_T = 2C_\gamma \frac{E^4 I}{e\rho}, \quad C_\gamma = \frac{4\pi}{3} \frac{r_e}{(m_e c^2)^3} = 8.86 \times 10^{-5} \text{ [m/GeV}^3\text{]} \quad (2.1)$$

Assuming that there are M_b bunches in each beam with bunch intensities N_b , the luminosity is

$$\mathcal{L} = \frac{f_{rev}}{4\pi} \frac{M_b N_b^2}{\sigma_x^* \sigma_y^*} \quad (2.2)$$

We will assume flat beams so that $\sigma_y^* \ll \sigma_x^*$. With this assumption, the vertical beam-beam tune shift is

$$\xi_y = \frac{r_e}{2\pi} \frac{N_b \beta_y^*}{\gamma \sigma_x^* \sigma_y^*} \quad (2.3)$$

Eliminating one power of N_b from the expression for the luminosity, we can write

$$\mathcal{L} = \frac{1}{2er_e} \frac{\xi_y}{\beta_y^*} \gamma I \quad (2.4)$$

I is the beam current in a single beam. Our strategy as stated earlier is that as we change parameters, P_T and ξ_y will be held constant.

Using Equation (2.4) to eliminate the current, we obtain the following equation for the luminosity and energy in terms of the fixed parameters and the bending radius ρ ,

$$\mathcal{L}\gamma^3 = \frac{3}{16\pi r_e^2 (m_e c^2)} \frac{\xi_y P_T}{\beta_y^*} \rho \quad (2.5)$$

This equation relates the parameters important to the physics program viz. the luminosity and energy to the machine size, optics and beam parameters. For example at constant luminosity, this equation shows that the maximum allowable energy increases only with the cube root of the radius, the radiated power or the beam-beam parameter. In the above equation β_y^* may be assumed constant at different energies only if the IR quadrupoles do not pose an aperture limitation in the vertical plane at any energy. We will assume that to be the case.

Similarly Equation (2.5) shows that the luminosity of the collider at a given energy and radiated power P_T can only be increased by increasing the beam-beam tune shift, ξ_y and/or lowering β_y^* . Other limits can however prevent the machine from operating at the maximum theoretical luminosity, for example, limits on the the maximum current in each bunch at injection.

2.1 Bunch intensity limitations

The dominant limitation on the bunch intensity at collision energy arises due to the beam-beam interactions. We have incorporated this constraint in our scaling of the luminosity with energy, Equation (2.5). Another limitation that is more severe at injection energy is the Transverse Mode Coupling Instability (TMCI). As in the classical head-tail instability, synchrotron motion which exchanges particles in the head and tail of the bunch drives the instability but this instability can arise even with zero chromaticity. In the presence of transverse impedances (typically wall resistivity), the wake forces excited by particles in the head can exert strong enough forces on the tail such that betatron modes $\omega_\beta + m\omega_s$ are modified. Typically, at the threshold intensity of the instability, the modes $m = 0$ and $m = -1$ become degenerate. TMCI is known to limit the bunch current in LEP to below 1 mA [4].

The threshold bunch current is given by

$$I_b^{TMCI} \simeq \frac{8f_{rev}\nu_s E}{e \sum_i \beta_i k_{\perp i}(\sigma_s)} \quad (2.6)$$

where ν_s is the synchrotron frequency, the sum in the denominator is over transverse impedances and $k_{\perp i}$ is a bunch length dependent transverse mode loss factor. Obviously higher synchrotron frequencies and longer bunches increase the threshold intensity. At LEP larger RF voltages are used to increase ν_s while emittance wigglers are used to increase the bunch length at the injection energy of 20 GeV. Compared to LEP, the very large lepton collider has a revolution frequency that is an order of magnitude smaller while the synchrotron frequency, injection energy and bunch length are comparable. If the impedances in LEP and this large ring are comparable, we may expect an order of magnitude reduction in the threshold current for this ring.

E. Keil[6] and G. Dugan[7] have done rough estimates of the threshold current for this large collider following the model of LEP. The dominant sources of broadband impedance will be the RF cavities, bellows and the resistive wall. LEP has bellows placed every 10 m around the ring. Assuming a similar placing and the same loss factors of the cavities and

bellows as in LEP, the loss factor in the bellows would be an order of magnitude larger than that in the cavities. At a bunch length of 1 cm the threshold current would reduce to around 0.01 mA. The number of bellows therefore should be kept to a minimum. Improvements in the vacuum system design may in fact allow the complete elimination of these bellows or at least to space them every km or so (see Section 10). In this case, the cavities and the resistive wall contribute about equally to the loss factor in this large ring. Dugan estimates that at an injection energy of 45 GeV (this will be discussed in Section 7) and in an elliptical chamber with aspect ratio of 2.5, the threshold current, I_b^{TMCI} , will be above 0.2 mA if the chamber half-height exceeds 4.8 cm. We will assume a design current of 0.1 mA to allow for a safety margin of 100%. It is worth noting that various schemes have been proposed to combat TMCI for the low-field hadron collider [8], e.g. starting with lower intensity bunches at injection energy and coalescing at higher energy, feedback systems etc. If required we may also use of one of these compensation schemes to allow a bunch current of 0.1 mA.

2.2 Beam intensity limitations

The available RF power determines the beam current to zeroth order. This constraint will be used in the design strategy in this report. However there are other sources of limitations which need to be considered as the design evolves. Perhaps the most important of these secondary limitations is the available cryogenic cooling power. We will assume that superconducting cavities will be used. The dynamic heat load on these cavities includes contributions from the RF dissipation and the beam induced heat load from both beams. These two sources lead to a power dissipation given by

$$P_{dynamic} = N_{cav} \frac{V_{RF}^2}{(R/Q)Q} + 2R_m(\sigma_s)I_b I_e \quad (2.7)$$

where N_{cav} is the number of cavities, (R/Q) is the normalized shunt impedance per cavity, Q is the unloaded quality factor of the cavities which depends on the operating temperature and the field gradient, R_m is a bunch length dependent loss impedance of the cavities, I_b is the bunch current, I_e is the single beam current. The available cryogenic power must be sufficient to cope with this load which has a contribution that increases with the beam current. The total higher order mode (HOM) power $P_{HOM} \propto I_b I_e$ that could be absorbed by the superconducting cavities was another restriction on the total beam current at LEP. An upgrade of the couplers and RF cables was required to cope with this limitation. Clearly the design of the cavities for the future lepton collider should take advantage of the experience gained while operating LEP.

2.3 Synchrotron radiation power and beam-beam limited regime

Here we specify the design strategy keeping the beam-beam parameter and the synchrotron radiation power constant. The beam-beam parameter depends on the bunch intensity while the power depends on the beam intensity. Hence we will determine the bunch intensity N_b from ξ_y and the number of bunches M_b from P_T while ensuring that the maximum bunch intensity stays below the threshold required to avoid the transverse mode coupled instability.

Writing the emittances in the transverse planes as

$$\epsilon_y = \kappa \epsilon_x$$

where κ is the coupling ratio, the bunch intensity can be expressed as

$$N_b = \left(\frac{2\pi}{r_e} \sqrt{\frac{\kappa\beta_x^* \xi_y}{\beta_y^*}} \right) \gamma \epsilon_x \quad (2.8)$$

where the factors within brackets are assumed to stay constant. One could imagine another scenario with optics changes where $\beta_x^*, \beta_y^*, \kappa$ are allowed to vary.

The equilibrium emittance ϵ_x is determined by the equilibrium between damping and quantum fluctuations and is given approximately by

$$\epsilon_x = \frac{C_q R \gamma^2}{J_x \rho \nu_x^3}, \quad C_q = \frac{55\hbar c}{32\sqrt{3}(m_e c^2)} = 3.83 \times 10^{-13}[\text{m}] \quad (2.9)$$

Here R is the average radius of the arc assumed to be made of periodic structures such as FODO cells and ν_x is the arc tune. If L_c, μ_c are the length of each periodic cell and the phase advance over the cell respectively, then

$$\nu_x = \frac{2\pi R \mu_c}{L_c 2\pi} = R \frac{\mu_c}{L_c} \quad (2.10)$$

Hence

$$\epsilon_x = \left(\frac{C_q R}{J_x \rho} \left[\frac{L_c}{\mu_c} \right]^3 \right) \frac{\gamma^2}{R^3} \quad (2.11)$$

The factor R/ρ - the ratio of the arc radius to the bend radius - can be treated as constant. Typically it has a value somewhere between 1.0 and 1.25. The arc radius is determined from the machine circumference C in terms of a filling factor f_1 . Thus

$$R = f_1 \frac{C}{2\pi}, \quad \text{and} \quad \rho = f_2 R, \quad f_1, f_2 < 1 \quad (2.12)$$

where f_1, f_2 are held constant. Since we do not make optics changes at different stages, we will treat the factor in brackets in Equation (2.11) as constant. The energy in this relation is of course determined from the energy luminosity relation Equation (2.5). Once the emittance is known, the bunch intensity is calculated from Equation (2.8).

The beam current I and the number of bunches are related as $I = e f_{rev} M_b N_b$, hence the maximum number of bunches is found from the total synchrotron radiation power as

$$M_b^{max} = \left(\frac{P_T}{2C_\gamma} \right) \frac{\rho}{f_{rev} N_b E^4} \quad (2.13)$$

The factors in brackets are constant while the other factors change with the machine circumference.

2.4 RF parameters

There are two requirements on the RF voltage parameters. The first requirement on the voltage is that the energy gained due to the RF per turn must equal to the energy lost per turn.

$$e V_{RF} \sin \phi_s = U = C_\gamma \frac{E^4}{\rho} \quad (2.14)$$

where $C_\gamma = (4\pi/3)r_e/(m_e c^2)^3 = 8.86 \times 10^{-5} \text{ m/GeV}^3$. The second requirement is that the RF acceptance ΔE_{RF} must be a certain number, say N_{QL} , times the rms energy spread σ_E for an acceptable quantum lifetime,

$$\Delta E_{RF} = N_{QL} \sigma_E \quad (2.15)$$

or

$$\sqrt{\frac{1}{\pi h \eta_{slip}} e V_{RF} E G(\phi_s)} = N_{QL} \sqrt{\frac{C_q}{J_s \rho} \frac{E^2}{m_e c^2}} \quad (2.16)$$

where

$$G(\phi_s) = 2 \cos \phi_s - (\pi - 2\phi_s) \sin \phi_s \quad (2.17)$$

J_s is the longitudinal damping partition number. Typically we require $N_{QL} \sim 10$. These two conditions can be solved to find the synchronous phase as the solution of the transcendental equation

$$\cot \phi_s + \phi_s - \frac{\pi}{2} - \frac{55\sqrt{3}}{256} \frac{h \eta_{slip}}{J_s \alpha_f} \frac{N_{QL}^2}{\gamma} = 0 \quad (2.18)$$

where $\alpha_f = e^2/(4\pi\epsilon_0 \hbar c) = 1/137.04$ is the fine structure constant. This equation can be solved numerically. Once the synchronous phase is known, the RF voltage can be found from Equation (2.14).

The RF frequency or the harmonic number is related to the desired bunch spacing. In order to accommodate both beams symmetrically around the ring, it is required that the bunch spacing be an even multiple of the RF wavelength. This in turn requires that the harmonic number be an even multiple of the number of bunches. The choice of RF frequency influences the energy acceptance $(\Delta E/E)_{accep}$ because $(\Delta E/E)_{accep} \propto 1/\sqrt{h}$ so lower RF frequencies increase the acceptance. However two economical factors argue for higher frequencies: (1) smaller frequencies increase the size and hence the cost of the cavity and (2) high power klystrons are more cost effective above frequencies of 300 MHz. In superconducting cavities the frequency is limited from above by several factors: (1) cavity losses increase with frequency, (2) longitudinal and transverse shunt impedances scale like ω_{RF} and ω_{RF}^2 respectively, (3) the ratio of the energy removed by a bunch from the cavity to the stored energy in the cavity also increases with frequency. In this paper we will consider RF frequencies in the neighbourhood of 400 MHz.

As an example, consider a circumference of 233km. We will develop a parameter list based on this circumference. We will assume a total synchrotron radiation power of 100 MW and a beam-beam parameter $\xi_y = 0.1 - 0.14$. The maximum number of bunches M_B^{max} determined by Equation (2.13) is 126. The revolution frequency is 1.315 kHz and the harmonic closest to 400 MHz is $310882 = 2 \times (15541)$. This does not have many divisors so a more convenient harmonic number is $310896 = 2 \times (4 \times 9 \times 17 \times 127)$. If we accept the requirement that $h = 2nM_B$, the allowed number of bunches less than M_B^{max} are all products of (2, 2, 2, 3, 3, 17) less than 126.

2.5 Optics

2.5.1 Arc optics

The choice of phase advance per cell μ_c and the length of a cell L_c are crucial design parameters. The equilibrium emittance decreases as the phase advance increases, reaches a

minimum at 135° and then increases again at larger values of μ_c . The horizontal dispersion also decreases with increasing phase advance and shorter cell lengths. Conversely, stronger focusing also increases the chromaticity and hence the strength of the sextupoles required to correct the chromaticity. Strong sextupoles can limit the available dynamic aperture. For these reasons, the choice of phase advance per cell in electron machines is usually limited in the range of $60^\circ \leq \mu_c < 120^\circ$. For example, LEP started operation with $(60^\circ, 60^\circ)$ phase advances in the (x, y) planes at 45 GeV, and since then has used $(90^\circ, 60^\circ)$, $(90^\circ, 90^\circ)$ and $(102^\circ, 90^\circ)$ phase advances at higher energies.

Another parameter affected by the choice of optics is the threshold current for TMCI. From Equation (2.6) we observe that $I_{thresh}^{TMCI} \propto \nu_s / (\sum_i \beta_i k_{\perp i})$. To estimate the dependence on μ_c, L_c we replace β_i by the average value in a FODO cell $\langle \beta \rangle = L_c / \sin \mu_c$. The synchrotron tune $\nu_s \propto \sqrt{\alpha_C}$ where α_C is the momentum compaction. Since $\alpha_C \propto 1 / \sin^2(\mu_c/2)$, we find

$$I_{thresh}^{TMCI} \propto \frac{\nu_s}{\langle \beta \rangle} \propto \frac{1}{L_c} \cos\left(\frac{\mu_c}{2}\right) \quad (2.19)$$

Hence the TMCI threshold is raised with shorter cell lengths and smaller phase advance per cell.

In this paper we will choose the phase advance per cell $\mu_c = 90^\circ$ and then choose a cell length L_c so that the bunch intensity does not exceed a certain threshold set by the TMCI. We will develop parameter sets (luminosity, energy, RF voltages,...) for different machine circumferences in this paper. As we increase the ring circumference μ_c, L_c will be assumed constant while the revolution frequency decreases and the bunch intensity always stays below the TMCI threshold.

The phase advance per cell is one way of controlling the equilibrium emittance. Another way is to redistribute the equilibrium emittance between the horizontal and longitudinal planes by changing the RF frequency. In a lattice constructed entirely of FODO cells, the change of partition number with momentum deviation is given by

$$\frac{dJ_x}{d\delta} = -\frac{dJ_s}{d\delta} = -4 \frac{L_D}{L_Q} \left[\frac{2 + \frac{1}{2} \sin^2 \mu_C/2}{\sin^2 \mu_C/2} \right] \quad (2.20)$$

where L_D, L_Q are the length of dipoles in a half cell and length of a quadrupole respectively. Writing $J_x(\delta) = J_x(0) + (dJ_x/d\delta)\delta + \dots$, we observe that reducing the emittance ϵ_x by half requires increasing the damping partition number to $J_x(\delta) = 2J_x(0)$ or a momentum shift of $\delta_{\Delta J_x=1} = 1/(dJ_x/d\delta)$ if initially $J_x(0) = 1$. The required RF frequency shift is related to the momentum deviation δ by

$$\frac{\Delta f_{RF}}{f_{RF}} = -\frac{\Delta R}{R} = -\alpha_C \delta \quad (2.21)$$

While the horizontal emittance can be changed by an appropriate shift in RF frequency, there is also a change in the radial excursion ΔR of the beam. It is important to keep this as small as possible both to minimize a loss in physical aperture and avoid a significant reduction in the transverse quantum lifetime. A lower phase advance per cell and a shorter quadrupole length relative to the dipole length, i.e. weaker focusing, help to keep the relative change in RF frequency and radial excursion small. As an example we consider the 233 km ring whose parameters will be given later in Section 6. With $L_D = 94.70$ m, $L_Q = 0.49$ m, $\mu_C = 90^\circ$, $\alpha_C = 0.23 \times 10^{-4}$, we find the damping aperture to be $\delta_{\Delta J_x=1} = 2.9 \times 10^{-4}$. The corresponding radial excursion is about $\Delta R = 0.20$ mm. Since this changes the damping

partition number by one, we can write this as the change in damping partition per unit of radial excursion,

$$\frac{\Delta J_x}{\Delta R} = 5.0 / [\text{mm}]$$

Thus radial excursions of the closed orbit by only fractions of a mm are sufficient to change the damping partition number by a unit or more.

An alternative method of reducing the transverse emittances is to place a damping wiggler in a region where the dispersion vanishes. Conversely the emittance could be increased if required, e.g. to reduce the beam-beam tune shift, by placing the wiggler where the dispersion is non-zero.

If the horizontal emittance is reduced by any method, the energy spread increases which decreases the energy resolution of the experiments and also the longitudinal quantum lifetime if the RF voltage is kept constant. This places constraints on the allowed emittance manipulations.

Synchrotron radiation in quadrupoles may be an issue. If the gradient is sufficiently large, then particles with large betatron amplitudes may radiate enough energy that they are lost from the RF bucket. This was termed the radiative beta-synchrotron coupling (RSBC) [9]. A rough measure of this effect [11] is the ratio of the field in a quadrupole at an amplitude equal to the rms beam size to the dipole bend field. To ensure that this effect is within bounds, the quadrupole gradient will be limited from above by requiring that this ratio not exceed unity.

2.5.2 Interaction Region

A detailed design of the IR must include the focusing scheme to obtain the desired spot sizes, a beam separation scheme, the collimation and masking scheme to protect components from synchrotron radiation, local chromaticity correction if required, the interface with the detectors etc. Here we will consider only the basic optics parameters. The lower limit on β^* , which could perhaps be 1 - 3 cm, is usually determined by the maximum tolerable beam size in the interaction region (IR) quadrupoles and the chromaticity generated by these quadrupoles. Furthermore to prevent the loss of luminosity due to the hourglass effect, β^* should be significantly greater than the bunch length. A preliminary IR design [12] shows that it is possible to achieve $\beta_y^* = 1$ cm with sufficient momentum aperture. A more precise estimate of the tolerable minimum requires tracking to determine the dynamic aperture of the machine with realistic arc and IR magnets.

Here we will assume that $\beta_y^* \ll \beta_x^*$ as is true at most $e^+ - e^-$ rings. Consequently aperture and chromaticity limitations will first arise in the vertical plane. As stated earlier in this section we will consider fixed values of β_x^*, β_y^* at all circumferences and energies and assume that these do not pose aperture restrictions at any energy. These values will need to be reconsidered during the design of the final focusing system.

The choice of β_y^*/β_x^* needs to be closely related to the emittance coupling ratio $\kappa = \epsilon_y/\epsilon_x$. The horizontal beam-beam parameter is related to the vertical parameter as

$$\xi_x = \left[\sqrt{\frac{\kappa}{\beta_y^*/\beta_x^*}} \right] \xi_y \quad (2.22)$$

If $\kappa > \beta_y^*/\beta_x^*$, then $\xi_x > \xi_y$. In this case the beam-beam limit is reached first in the horizontal plane. Beyond this limiting current, the emittance grows linearly with current and

the beam-beam parameters stay constant. In particular the vertical beam-beam parameter ξ_y never reaches its maximum value and since the luminosity is proportional to ξ_y , the maximum luminosity is not obtained. It is therefore desirable to have $\kappa \leq \beta_y^*/\beta_x^*$. In this paper we will consider the so called *optimal coupling* scenario where $\kappa = \beta_y^*/\beta_x^*$ and the beam-beam limits are attained simultaneously in both planes, $\xi_x = \xi_y$.

2.6 Summary of design strategy

The design of the ring optics depends on a number of parameters, among these are the maximum synchrotron radiation power allowed by the facility, the maximum beam-beam parameter which is assumed, the number of IPs required to satisfy the user community (and saturate the tolerable beam beam tune shift), the maximum bunch intensity limited by TMCI. In addition the minimum beta functions at the interaction point, β_x^*, β_y^* , the emittance coupling ratio $\kappa = \epsilon_y/\epsilon_x = \beta_y^*/\beta_x^*$, must be specified. The arc design is determined by the arc filling factor f_1 and ring filling factor f_2 , which can be realized in a realistic design, the phase advance per cell μ_C , and the required rf voltage determined by N_{QL} - the ratio of RF bucket height (energy acceptance) to rms energy spread.

The design values for a first iteration can be produced from these requirements. For a given machine circumference C , determine the bend radius ρ and arc radius R from Equation (2.12) with assumed values of f_1, f_2 . The maximum energy of the ring at this circumference can then be determined from Equation (2.5). The equilibrium emittance at this energy and required maximum bunch intensity from Equation (2.8) can be calculated and compared with the maximum bunch current allowed by I_{thresh}^{TMCI} . The cell length can be obtained from Equation (2.11). The maximum number of bunches can be obtained from Equation (2.13). The maximum quadrupole gradient tolerable B'_{max} is found from

$$\frac{B'_{max}\sigma_x}{B_0} = 1$$

where σ_x is the rms horizontal beam size in the arcs and B_0 is the bend field. The values obtained must then be checked for internal consistency and collider performance.

3 Lifetime

The radiative Bhabha scattering process $e^+e^- \rightarrow e^+e^-\gamma$ is expected to dominate the beam lifetime at collision in this large lepton collider. The lifetime from this process with a scattering cross-section $\sigma_{e^+e^-}$ is

$$\tau_L = \frac{1}{N_{IP}} \frac{M_b N_b}{\mathcal{L} \sigma_{e^+e^-}} \quad (3.1)$$

Substituting for the luminosity from Equation (2.4) we can write this in terms of the beam-beam parameter ξ_y as

$$\tau_L = \left[\frac{2r_e}{N_{IP}} \frac{\beta_y^*}{\xi_y} \frac{1}{\sigma_{e^+e^-}} \right] \frac{1}{\gamma f_{rev}} \quad (3.2)$$

The cross-section $\sigma_{e^+e^-}$ has a weak logarithmic dependence on energy (see Equation (A.25) in Appendix A) which can be ignored to first order. Assuming that β_y^*, ξ_y are constant, the terms in square brackets above can be considered nearly constant. At a fixed circumference, the luminosity lifetime decreases with approximately the first power of the energy.

There are other contributions to the beam lifetime such as beam-gas scattering and Compton scattering off thermal photons but those lifetimes are about an order of magnitude larger than the luminosity lifetime considered above. For present purposes those effects can be ignored but need to be considered at a later stage.

4 Scaling of the beam-beam parameter

Although a value of the beam-beam tune shift of $\xi_x \sim \xi_y \sim 0.03 - 0.06$ has described the operation of almost all lepton colliders over the past 20 years, recent results at LEP have shown that large colliders at high energies behave somewhat differently. The LEP machine operated quite reliably at tune shifts around $\xi_x \sim \xi_y \sim 0.09$, [4] and, in fact, was limited by the transverse mode coupling instability rather than the beam beam tune shift, which was estimated to be in the range of 0.14 [11]. Since the machine described here is even larger and higher energy than LEP, we consider how the LEP tune shifts can be extrapolated, and ultimately consider a maximum tune shift in the range of 0.17 for normal operation at the highest energies.

The damping time τ_s determines the time it takes for the beam to reach an equilibrium distribution in the absence of external nonlinear forces. As the damping increases and this time decreases, the beam becomes more immune to non-resonant perturbations that would change this equilibrium distribution. Indeed observations at several $e^+ - e^-$ colliders have shown that the limiting value of the beam-beam parameter increases slowly with energy or more precisely with the damping decrement. The damping decrement for beam-beam collisions is defined as the inverse of the number of beam-beam collisions per damping period,

$$\lambda_d = \frac{1}{N_{IP}\tau_s} \quad (4.1)$$

where τ_s is the damping time measured in turns. For example at LEP, the beam-beam limit has increased by more than 50% as the energy was increased from 45.6 GeV to nearly 100 GeV. Fitting a power law to the LEP data [4] for the maximum beam-beam tune shifts at three different energies we find that

$$\xi_{y,max} \sim \lambda_d^{0.26} \quad (4.2)$$

Earlier Keil and Talman [13] and more recently Peggs [10] considered the scaling of the beam-beam tune shift with λ_d applied to data from earlier machines such as SPEAR, PETRA, CESR and found roughly the same power law behaviour. Figure 1 shows this power law curve and also the expected beam-beam tune shifts for VLLC33 and VLLC34. The damping decrement for VLLC33 at 185 GeV is 0.01 which implies $\xi_{y,max} = 0.1$ while for VLLC34 where the maximum energy is lower, $\lambda_d = 0.0006$ and the expected $\xi_{y,max} = 0.05$. Uncertainties in the data and the fitting of this data to a power law may in fact allow higher values in the range $0.1 \leq \xi_{y,max} \leq 0.14$ at 185 GeV [11].

5 Polarization

In a storage ring electrons become vertically polarized via the emission of synchrotron radiation. In a perfect ring - planar and without errors - this polarization would build up to a maximum value of 92.4%. In a real ring - nonplanar, misalignments and field errors - the maximum achievable polarization can be significantly less. The emission of photons with

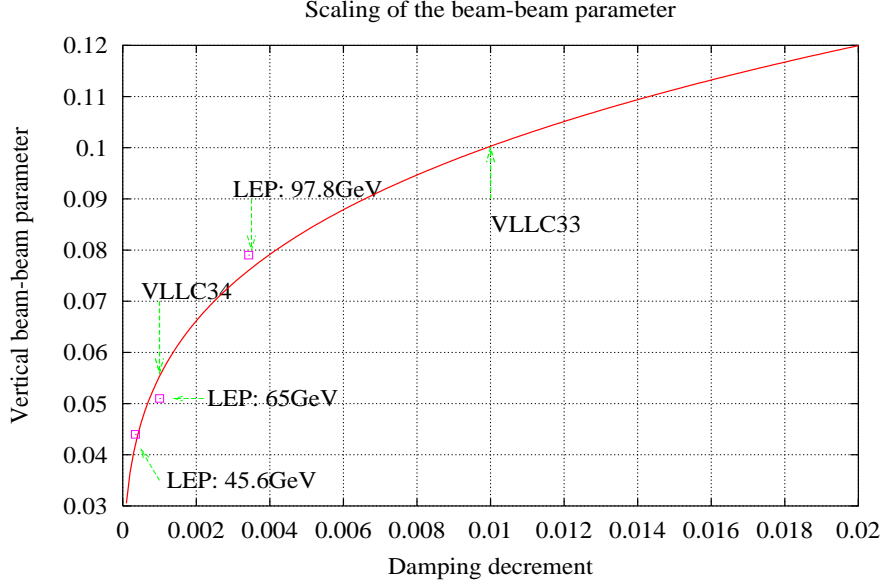


Figure 1: The LEP data on the maximum beam-beam tune shift is fit to a power law curve. Also shown are the damping decrements and expected maximum beam-beam parameter for the VLLC33 (luminosity= $10^{33} \text{ cm}^{-2} \text{ sec}^{-1}$) and VLLC34 (luminosity= $10^{34} \text{ cm}^{-2} \text{ sec}^{-1}$) design parameters.

a very small probability of spin flip while leading to polarization also leads to depolarization in the presence of imperfections. The stochastic changes in electron energy after photon emission and coupling to the orbit motion lead to spin diffusion and loss of polarization. In the presence of depolarizing effects, the maximum value of the polarization along the equilibrium spin direction \hat{n} is given by the expression due to Derbenev and Kondratenko

$$P_{\infty} = -\frac{8}{5\sqrt{3}} \frac{\oint ds \langle \frac{1}{|\rho(s)|^3} \hat{y} \cdot (\hat{n} - \partial\hat{n}/\partial\delta) \rangle_s}{\oint ds \langle \frac{1}{|\rho(s)|^3} [1 - \frac{2}{9}(\hat{n} \cdot \hat{s})^2 + \frac{11}{18}(\partial\hat{n}/\partial\delta)^2] \rangle_s} \quad (5.1)$$

where $\delta = \Delta p/p$ and $\langle \rangle_s$ denotes the average over phase space at a location s . We note that \hat{n} is a vector field which changes with location in phase space. The polarization rate is approximately [14]

$$\frac{1}{\tau} = \frac{1}{\tau_{ST}} + \frac{1}{\tau_{Dep}} \quad (5.2)$$

$$\frac{1}{\tau_{ST}} = \frac{8}{5\sqrt{3}} \frac{e^2 \gamma^5 \hbar}{m_e^2 c^2 C} \oint ds \langle \frac{1}{|\rho(s)|^3} [1 - \frac{2}{9}(\hat{n}_0 \cdot \hat{s})^2] \rangle_s \quad (5.3)$$

$$\frac{1}{\tau_{Dep}} = \frac{8}{5\sqrt{3}} \frac{e^2 \gamma^5 \hbar}{m_e^2 c^2 C} \oint ds \langle \frac{1}{|\rho(s)|^3} \frac{11}{18} (\partial\hat{n}/\partial\delta)^2 \rangle_s \quad (5.4)$$

When \hat{n}_0 is nearly vertical, then $\hat{n}_0 \cdot \hat{s}$ is small compared to unity and assuming that the bend radius is everywhere the same, the Sokolov-Ternov polarization rate reduces to the simplified expression

$$\frac{1}{\tau_{ST}} \approx \frac{8}{5\sqrt{3}} \frac{e^2 \hbar}{m_e^2 c^2} \frac{\gamma^5}{\rho^3} \quad (5.5)$$

The time to build up to the asymptotic polarization falls sharply with increasing energy but increases as the cube of the bend radius. The energy ratio between this collider and LEP is between two to three while the radius is nearly an order of magnitude larger than LEP. Consequently the polarization build up time in this machine will be a few hours compared to approximately 6 minutes at 100 GeV in LEP. Polarization may still be a practical possibility but that is primarily determined by the value of the achievable asymptotic polarization.

The key to calculating the asymptotic polarization P_∞ in a real machine lies in the calculation of the spin-orbit coupling vector $\partial\hat{n}/\partial\delta$. This depends on the detailed lattice configuration and there are several sophisticated programs which do this [14, 15].

Observations at several $e^+ - e^-$ rings have shown that the maximum polarization drops with energy. For electrons, integer resonances are spaced 0.44 GeV apart so the larger energy spread at higher energies leads to a larger portion of the resonance to be spanned by the beam distribution. However prediction of the drop in polarization with energy is complicated and there does not exist a simple analytical way to extract the energy dependence of \hat{n} in general. If however we assume that both orbital and spin motion is approximately linear, then examination of the spin-orbit coupling matrices (the \mathbf{G} matrices in [14]) shows that $\partial\hat{n}/\partial\delta \propto \gamma^2$. Using Equation (5.1) this implies [16] that the asymptotic polarization scales as

$$P_\infty = \frac{8}{5\sqrt{3}} \frac{1}{1 + \beta E^4} \quad (5.6)$$

Here β is a parameter which does not depend on energy. Experience has shown that this relation is nearly true if the motion is linear and the closed orbit is well corrected. This scaling law will be violated if either the orbital motion or the spin motion is strongly nonlinear. Observations at LEP show a sharp fall off in polarization above 45 GeV and polarization at the level of a few % at 60 GeV. This would predict that there will be no usable polarization at the energies of interest in this very large ring.

It may however be possible to increase the polarization by a combination of methods, as used for example in HERA [17]. These include:

- Tight alignment tolerances on all magnets, specially in the vertical plane.
- Extremely good correction of the vertical closed orbit distortions and the vertical dispersion.
- Careful selection of the tunes, e.g. the energy should be chosen so that the fractional part of the spin tune (approximately equal to $a\gamma$) is close to 0.5. At energies near 185 GeV, this would specify an energy of 184.84 GeV. The tunes in all planes should be chosen so that the resonance conditions

$$\nu = k + m_x\nu_x + m_y\nu_y + m_s\nu_s$$

are far from satisfied especially for 1st order resonances $|m_x| + |m_y| + |m_s| = 1$ and low order synchrotron sideband resonances of 1st order betatron resonances $|m_x| + |m_y| = 1$.

- Harmonic spin matching and minimizing the spin orbit coupling will be essential. A sequence of vertical orbit correctors and dispersion correctors is used to generate harmonics which compensate the integer and linear spin resonances driven by the imperfection fields. These correction methods can be facilitated by making each section of the ring locally “spin transparent” which would place constraints on the phase advances and other Twiss functions in these sections.

It is clear that if polarization is desired, the lattice must be designed from the outset to achieve this. Further studies are required however to examine whether, even with the use of the methods outlined above, respectable levels of polarization will be achievable at the energies of interest.

6 Design Parameters at High Energy

The design strategy has been outlined in Section 2. We know for example that at fixed luminosity, synchrotron radiation power and beam-beam parameter that the maximum energy of the beams scales with the cube root of the circumference. Here we apply this strategy to different machines with circumferences in the range from 200 km to 300 km. This should span the range envisioned for different versions of the VLHC.

One feature of the design that needs some iteration is the initial choice of the beam-beam parameter. We have seen in Section 4 that the maximum beam-beam parameter scales with some power of the energy. Since the beam energy is an output parameter, we need to ensure that the choice of the beam-beam parameter is self-consistent with the design energy.

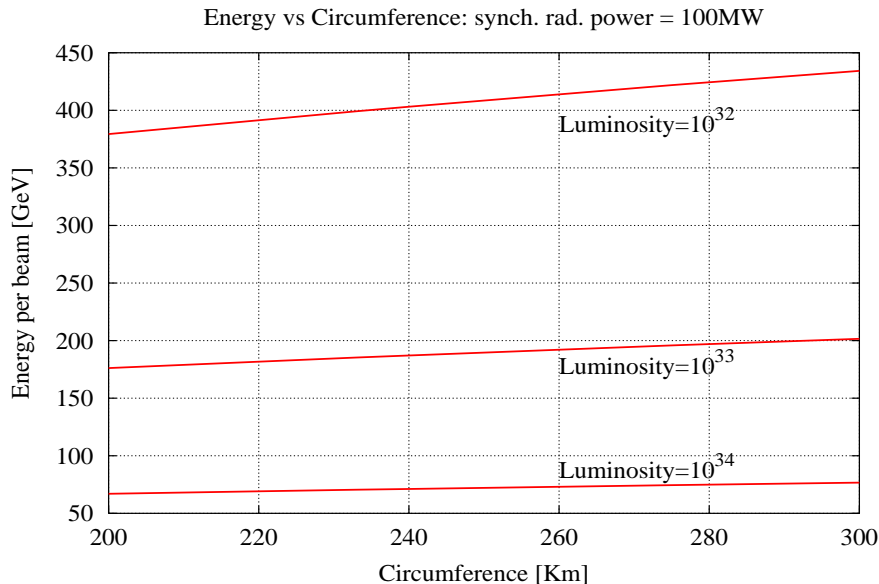


Figure 2: The maximum energy attainable as a function of the machine circumference for three different luminosities. At the energies obtainable with luminosities of $10^{33} \text{ cm}^{-2} \text{ sec}^{-1}$ and lower, the maximum beam-beam parameter was set to 0.1. At the luminosity of $10^{34} \text{ cm}^{-2} \text{ sec}^{-1}$, the beam-beam parameter was set 0.05. The synchrotron radiation power of both beams was set to 100MW in all cases.

Figure 2 shows the maximum energy as a function of the circumference for three different luminosities. For example at a circumference of 233 km, the maximum single beam energies at luminosities of 10^{32} , 10^{33} , $10^{34} \text{ cm}^{-2} \text{ sec}^{-1}$ are 396, 185 and 70 GeV respectively. Thus a ring with circumference around 233 km should suffice to reach the top quark production threshold, estimated to be at 360GeV, with a luminosity close to $10^{33} \text{ cm}^{-2} \text{ sec}^{-1}$. One also observes that single beam energies from 300-500 GeV appear attainable at a luminosity of $10^{32} \text{ cm}^{-2} \text{ sec}^{-1}$. However the RF voltages required in this range of energies is in the

hundreds of GV as seen in Figure 3. In the range of 150-250 GeV per beam and luminosity $10^{33} \text{ cm}^{-2}\text{sec}^{-1}$, the RF voltages are a few GV, comparable to LEP.

Figure 4 shows the $e^- - e^+$ bremsstrahlung lifetime as a function of circumference at three luminosities. We observe that at a luminosity of $10^{33} \text{ cm}^{-2}\text{sec}^{-1}$, this lifetime ranges from 15-36 hours which should be adequate considering that this is the dominant contribution to the beam lifetime at luminosity. The lifetime was calculated using the expression (A.25) for the bremsstrahlung cross-section which does not have corrections from a cut-off parameter which corresponds to the characteristic distance between particles in the bunches. With this cut-off the cross-sections are typically 30% lower. For example analysis of the cross-section at LEP energies [31] showed that the uncorrected cross-section of 0.3 barns was reduced to 0.2 barns. This number was found to agree well with measurements. As a consequence of the smaller cross-section, luminosity lifetimes may be about 30% higher than shown in Figure 4. At most energies, the lifetime is typically in the tens of hours and increases to hundreds of hours when the energy drops to less than 100 GeV as is the case when the required luminosity is $10^{34} \text{ cm}^{-2}\text{sec}^{-1}$. By comparison, the luminosity lifetime at LEP is about 5-6 hours.

Table 1 shows the design parameters of a 233 km ring obtained by following the design strategy outlined in Section 2. We remark on some of the interesting features of this ring compared to LEP.

- Increasing the circumference of LEP by a factor of 8.5 and the total synchrotron radiation power by about 7 allows a 10 fold increase in luminosity at almost double the energy.
- The bunch current in VLLC33 is roughly 7 times lower in keeping with the expected lower threshold for TMCI.
- The $e^+ - e^-$ bremsstrahlung lifetime in VLLC33 is significantly longer at 23 hours.
- The vertical beam sizes in the two machines are comparable
- The horizontal beams sizes in the arcs of the two machines are also close. Hence vacuum chamber dimensions in VLLC33 can be similar to those in LEP.
- The main dipole field is about 5 times weaker than that of LEP. Iron magnets operated at room temperature will suffice. Conversely, good shielding from stray magnetic fields, e.g. those of the low field hadron collider, will be critical.
- The critical energy is smaller in VLLC33 so shielding against synchrotron radiation as in LEP should be adequate for VLLC33. The photon flux per unit length is almost the same in the two machines.
- The RF voltage required for VLLC33 is significantly higher at 4.7GV (without beam loading) compared to 3.1GV (presumably with beam loading) for LEP.
- We assumed $f_1 = f_2 = 0.84$ to have the same ratio of bend radius ρ to the machine radius $C/(2\pi)$ as in LEP. A somewhat more aggressive choice of packing fractions $f_1 = f_2 = 0.90$ or $2\pi\rho/C = 0.81$ yields slightly different parameters, e.g. maximum energy $E_{max} = 193 \text{ GeV}$, RF voltage $V_{RF} = 4883 \text{ MV}$. Both of these quantities scale with the third root of the bend radius.
- We chose optimum coupling, i.e. $\epsilon_y/\epsilon_x = \beta_y^*/\beta_x^*$ which implies that $\xi_x = \xi_y$. Operating at the beam-beam limit in both planes might well be challenging. If we reduce the emittance coupling to half this value, $\epsilon_y/\epsilon_x = 0.025$, then $\xi_x = 0.071$ while staying at the beam-beam limit in the vertical plane $\xi_y = 0.1$. With this choice, optics and

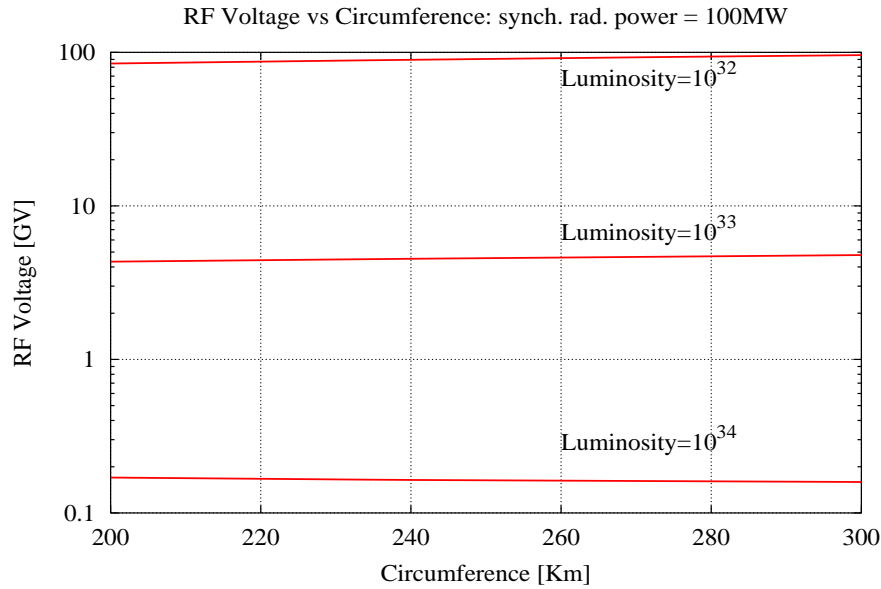


Figure 3: RF voltage required when operating at the maximum energy as a function of the machine circumference for different luminosities with the synchrotron radiation power of both beams set to 100MW in all cases.

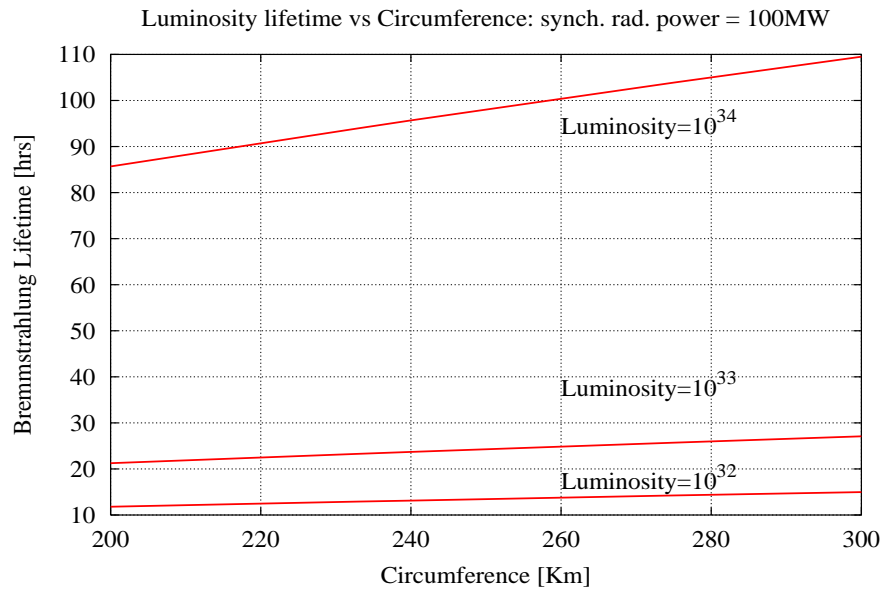


Figure 4: Luminosity lifetime vs the circumference at three different luminosities. Here the lifetime *increases* with the required luminosity because the maximum energy decreases at higher luminosities and the lifetime $\sim 1/E$, cf. Equation(3.2). See the text for other remarks.

$e^+ - e^-$ Collider Parameters

Parameter	LEP 1999	VLLC33
Circumference [m]	26658.9	233000.
β_x^*, β_y^* [cm]	150, 5	100, 5
$\kappa / (\beta_y^* / \beta_x^*)$	0.31	1.0
Luminosity [$\text{cm}^{-2}\text{sec}^{-1}$]	9.73×10^{31}	1×10^{33}
Maximum Energy [GeV]	97.8	185.3
Emittances ϵ_x, ϵ_y [nm]	21.1, 0.220	6.06, 0.30
RMS Beam size at IP σ_x^*, σ_y^* [μm]	178., 3.30	77.52, 3.88
Bunch intensity/current [/mA]	$4.01 \times 10^{11} / 0.720$	$4.85 \times 10^{11} / 0.10$
Number of bunches per beam	4	126
Bunch spacing [km]	6.66	1.85
Total beam current (both beams) [mA]	5.76	25.20
Beam-beam tune shift ξ_x, ξ_y	0.043, 0.079	0.1, 0.1
e^+e^- bremsstrahlung lifetime [hrs]	6.0	23.6
Dipole field [T]	0.110	0.0238
Bend Radius [m]	3026.42	25968.1
Phase advance per cell μ_x, μ_y [degrees]	102, 90	90.0
Arc tune	70.3, 62.0	215
Cell Length [m]	79.110	226.345
Total length of dipoles in a cell [m]	69	189.41
Quadrupole gradient [T/m]	9.50	15.59
Length of a quadrupole [m]	1.60	0.494
Arc β^{max}, β^{min} [m]	144, 18	386, 66
Arc $\sigma_x^{max}, \sigma_x^{min}$ [mm]	1.70, 0.60	1.52, 0.63
Arc dispersion D^{max}, D^{min} [m]	1.03, 0.450	1.12, 0.53
Bend radius to Machine radius $2\pi\rho/C$	0.710	0.70
Momentum compaction	1.60×10^{-4}	2.23×10^{-5}
Polarization time [hrs]	0.1	2.2
Energy loss per particle per turn [GeV]	2.67	4.0
Critical energy [keV]	686.	452.61
Longitudinal damping time [turns]	73.0	46.3
RMS relative energy spread	1.52×10^{-3}	9.83×10^{-4}
Bunch length [mm]	11.0	7.06
Synchrotron tune	0.116	0.115
RF Voltage [MV]	3050.00	4572.5
RF frequency [MHz]	352.209	400.
Revolution frequency [kHz]	11.245	1.287
Synchrotron radiation power - both beams [MW]	14.5	100.7
Available RF power [MW]	34.1	
Power load from both beams [kW/m]	0.820	0.517
Photon flux/length from both beams [/m/sec]	2.40×10^{16}	1.15×10^{16}

Table 1: Parameters of the very large lepton collider with a desired luminosity of $10^{33} \text{ cm}^{-2}\text{sec}^{-1}$ and a circumference of 233km.

beam size parameters change, e.g. $\epsilon_x = 11.8$ nm, cell length=278 m, $\beta^{max} = 475$ m, $D_x^{max} = 1.72$ m, $\sigma_x^{max} = 2.4$ mm, $\nu_s = 0.156$, $\sigma_l = 8.1$ mm. The RF voltage increases to 4780 MV while most other parameters are relatively unaffected.

- We chose an energy acceptance that is ten times the equilibrium energy spread of the beam to ensure sufficient quantum lifetime. At LEP with the parameters given in Table 1, this ratio is only about 6.6. If we assume this value for the 233 km ring, the RF voltage is lowered from 4.57 GV to 4.43 GV. The energy loss per turn requires that the RF voltage be greater than 4 GV.

7 Operation at 45 GeV

There is considerable interest in precision measurements at the W and Z^0 mass range, $E_{CM} \sim 90$ GeV. Here we consider the feasibility of using this large collider to attain high luminosities - in excess of $5 \times 10^{33} \text{ cm}^{-2} \text{ sec}^{-1}$. These are the so-called ‘‘gigaZ’’ measurements which required integrated luminosities around 500 inverse picobarns. Polarized beams at this energy will greatly add to the physics program allowing for example measurements of the left right asymmetry or the Weinberg angle.

The design principles for obtaining high luminosity at low energies are different from those at high energy. At low energies, the synchrotron radiation power is low and does not impose any constraints. Only the beam-beam tunes shift limit needs to be respected. This constrains the bunch intensity per unit transverse area or N_e/ϵ . Under these conditions, the luminosity is

$$\mathcal{L} = \frac{\pi}{r_e^2} M_B f_{rev} \left[\frac{\sigma_x^* \sigma_y^*}{(\beta_y^*)^2} \right] \gamma^2 \xi_y^2 \quad (7.1)$$

$$= \frac{\pi}{r_e^2} M_B f_{rev} \left[\frac{\kappa \beta_x^*}{(\beta_y^*)^3} \right]^{1/2} \gamma^2 \xi_y^2 \epsilon_x \quad (7.2)$$

In this regime the luminosity increases with the emittance $\mathcal{L} \propto \epsilon_x$ so this requires that the aperture be filled to maximize the luminosity. Leaving enough room for good quantum lifetime, the maximum permissible emittance could be determined by a condition such as

$$A_{req} \equiv 10 * [\sigma_x^2 + (D_x \delta_p)^2]^{1/2} + \text{c.o.d} \leq r_{pipe} \quad (7.3)$$

where c.o.d is the expected closed orbit distortion and r_{pipe} is the radius of the beam pipe. The emittance can be increased by lowering the phase advance per cell. The bunch intensity is found from the beam-beam tune shift

$$N_b = \left(\frac{2\pi}{r_e} \sqrt{\frac{\kappa}{\beta_y^* / \beta_x^*}} \right) \gamma \epsilon_x \xi_y \quad (7.4)$$

If this intensity exceeds the TMCI threshold N_b^{TMCI} , the emittance can be lowered by increasing the phase advance.

There is no significant constraint on the beam current from the synchrotron radiation power so this does not limit the number of bunches. Instead the number of bunches is limited by the minimum bunch spacing allowed. This spacing S_b^{min} could be limited by multi-bunch instabilities. Assuming a uniform bunch distribution around the ring, the number of bunches is determined by

$$M_B f_{rev} = \frac{c}{S_b^{min}} \quad (7.5)$$

We will assume $S_b^{min} = 5$ m, somewhat arbitrarily. It remains to be checked that this short a bunch spacing is feasible with a reasonable longitudinal feedback system.

For 45 GeV operation we will use the same magnet lengths as determined by high energy operation. The cell length is also fixed although it may be attractive to double the cell length by turning off half (or perhaps two thirds of) the quadrupoles. This would allow a higher phase advance for the same emittance. We assume that the beam pipe radius is 5 cm. The parameters that are determined by high energy operation are shown in Table 2.

Circumference [km]	233.00
Revolution frequency [kHz]	1.2867
Arc radius [m]	31031.880
Bend radius [m]	25968.098
β_x^*, β_y^* [cm]	100.0, 5.0
Ratio of emittances	0.050
Number of cells	861
Bend angle in half-cell [mrad]	3.647
Length of cell [m]	226.345
Length of all dipoles in cell [m]	189.410
Quadrupole length [m]	0.494
Cell packing fraction	0.189

Table 2: Fixed parameters for 45 GeV operation. These are determined by optimizing at 185 GeV.

The minimum phase advance per cell μ^{min} is determined by the requirement $A_{req} \leq 5$ cm. We allow for a rms closed orbit distortion of 1 cm - a conservatively large value. The left figure in Figure 5 shows the emittance and A_{req} as a function of the phase advance. From this figure we determine $\mu^{min} = 25^\circ$. The right figure in Figure 5 shows that the luminosity drops below $10^{34} \text{ cm}^{-2}\text{sec}^{-1}$ at phase advances greater than 27° . Hence we set the phase advance per cell to the minimum value $\mu_C = \mu^{min}$. The values of other parameters follow and are shown in Table 3.

The luminosity is slightly above $10^{34} \text{ cm}^{-2}\text{sec}^{-1}$. This theoretical value will correspond to the peak luminosity at best. A more aggressive design will be necessary if the average luminosity is required to be $10^{34} \text{ cm}^{-2}\text{sec}^{-1}$. The single bunch current is low at 0.03 mA or about a third of that required at 185 GeV so the TMCI instability may not be an issue. However with the large number of bunches, the beam current is high at 1.4 A. This makes the design more akin to that of the B factories. While the RF voltage required is low at 50 MV, we assume that it will be provided by the superconducting cavities required for operation at 185 GeV. The dynamic heat load and the HOM power generated in these cavities may be substantial at these high beam currents and may therefore rule out such a large beam current. Multi-bunch instabilities may also be severe and therefore require dedicated feedback systems for low energy operation. Finally the Sokolov-Ternov polarization time is 2600 hours, thus physics with polarized beams is not an option at this energy unless one injects polarized beams into the ring.

In short, operation at 45 GeV will require several different challenges to be faced compared to operation at 185 GeV. It is not even clear if the components will be able to withstand

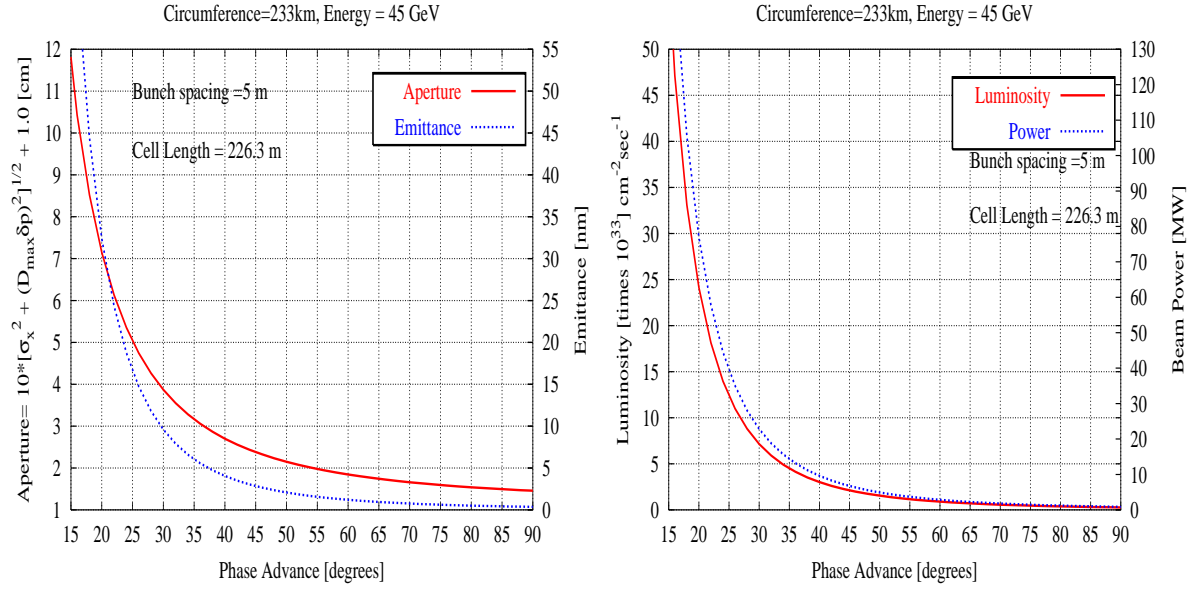


Figure 5: Left: The emittance and A_{req} as a function of the phase advance per cell. Assuming the beam pipe radius is 5 cm, this determines the phase advance to be 25° . Right: The luminosity and synchrotron radiation power as a function of the phase advance. The luminosity drops below $10^{34} \text{ cm}^{-2}\text{sec}^{-1}$ at phase advances greater than 27° .

the high beam currents required. Therefore it makes more sense to consider a smaller ring for physics at the Z0 mass. A natural choice for this would be the injector to the large ring. Such a ring (a Z0 factory) has been proposed by E. Keil [6]. The top energy of this injector is 45 GeV with a circumference of 12.57 km chosen so that the polarization time is reasonable at about 20 minutes. Besides the physics potential of this ring, this is an attractive option for several other reasons. It raises the injection energy into the VLLC and thus may alleviate or eliminate concerns about TMCI in the large ring. Also it would allow physics to be possible while the VLLC is under construction.

Energy [GeV]	45.00
Luminosity	12.38×10^{33}
Synch. radiation power(both beams) [MW]	39.40
σ_x^*, σ_y^* [microns]	128.8, 6.4
Number of bunches	46600
Bunch spacing [km]	0.0050
Particles per bunch	1.47×10^{11}
Bunch current [mA]	0.0302
Emittances [nano-m]	16.59, 0.83
Beam-beam parameter	0.045
Damping decrement	0.00016
Single beam current [mA]	1408.08
Brho [Tesla-m]	150.10
Arc tune	59.8
Phase advance per cell [deg]	25.0
Dipole field [T]	0.00578
Focal length of cell [m]	261.44
Quad gradient [T/m]	1.161
Quad field at $1\sigma_x^{max}$ /dipole field	0.66
Cell: β_{max}, β_{min} [m]	651.50, 419.66
Cell: $\sigma_x^{max}, \sigma_x^{min}$ [mm]	3.29, 2.64
Cell: $\sigma_y^{max}, \sigma_y^{min}$ [mm]	0.74, 0.59
Max apertures required [cm]	5.03, 1.74
Max and min disp. [m]	9.76, 7.86
Momentum compaction	0.2376×10^{-3}
Energy loss per turn [GeV]	0.014
Damping time [turns]	3216
RF Voltage [GV]	0.05
Synchronous phase [deg]	16.25
Relative energy spread	0.239×10^{-3}
RF acceptance	0.240×10^{-2}
Synchrotron tune	0.112
Bunch length [mm]	18.82
Longitudinal emittance [eV-sec]	0.0021
Bremm. cross-section [barns]	0.454
Bremm. lifetime [hrs]	168.9
Polarization time [hrs]	2600.8
Critical energy [keV]	6.514
Critical wavelength [Å]	1.593
Number of photons/m/sec	0.314×10^{18}
Gas load [torr-L/m-sec]	0.282×10^{-6}
Linear Power load(both beams) [kW/m]	0.202

Table 3: Parameters of a 45 GeV ring with the same circumference and magnets as the 185 GeV ring with parameters in Table 1.

Parameter	Energy dependence
Equilibrium emittance ϵ_x	γ^2
Energy loss U_0 , RF Voltage V_{RF}	γ^4
Damping time $\tau_s \sim E/U_0$	γ^{-3}
Maximum beam-beam parameter $\xi_y \sim \tau_s^{-0.26}$	$\gamma^{0.8}$
Luminosity $\mathcal{L} \sim \xi_y \gamma^{-3}$	$\gamma^{-2.2}$
Bunch intensity $N_b \sim \xi_y \gamma \epsilon_x$	$\gamma^{3.8}$
Maximum number of bunches $M_B^{max} \sim 1/(N_b E^4)$	$\gamma^{-7.8}$
Synchrotron frequency ν_s	$\gamma^{3/2}$
Equilibrium energy spread σ_E/E	γ
Bunch length σ_l	$\gamma^{-1/2}$
Critical energy E_c	γ^3
Bremmstrahlung lifetime $\tau_L \sim 1/(\xi_y \gamma)$	$\gamma^{-1.8}$

Table 4: Scaling of beam parameters with energy. Machine circumference and synchrotron radiation power are kept fixed.

8 Scaling Laws with Energy

In the previous two sections we developed parameter sets for operation at 185 GeV and 45 GeV respectively. The design philosophies at these two energies were quite different. The main interest in this ring however is at the high energy end so it is important to determine the useful upper limit in energy for this machine. Thus for all energies above 100 GeV or so, the design philosophy outlined in Section 2 is relevant.

We assume that magnet lengths, phase advances are chosen at some energy of interest and thereafter kept fixed. Table 4 shows the scaling with energy of some of the important parameters. Most of these dependences on energy are well known. For example the equilibrium emittance increases as γ^2 and the RF voltage increases as γ^4 . The additional twist here is that the beam-beam parameter is allowed to scale with energy and recent data (see Section 4) suggest that in a given machine $\xi_y^{max} \sim \gamma^{0.8}$. If we are to operate at the beam-beam limit at all energies, then (a) the luminosity drops more slowly with energy $\mathcal{L} \sim \gamma^{-2.2}$ compared to γ^{-3} without the scaling of the beam-beam parameter and (b) the bunch intensity increases more rapidly as $N_b \sim \gamma^{3.8}$ rather than γ^3 . The $e^+ - e^-$ bremsstrahlung lifetime also drops faster with energy as $\tau_L \sim \gamma^{-1.8}$ in this scenario.

Figure 6 shows the values of luminosity and RF voltage as a function of energy with a ring circumference of 233 km and synchrotron radiation power kept constant at 100 MW. As mentioned above ξ is allowed to scale with energy and the values at some of the energies are shown in the figure. On this plot we show the luminosity and RF voltage at 45 GeV as a single data point while the values above 100 GeV are obtained using the high energy design strategy. We observe that if a maximum of 15 GV of RF is available, the energy reach of a single beam in this ring extends from 100 GeV to 250 GeV with luminosities in the range from $0.5-4 \times 10^{33} \text{ cm}^{-2} \text{ sec}^{-1}$.

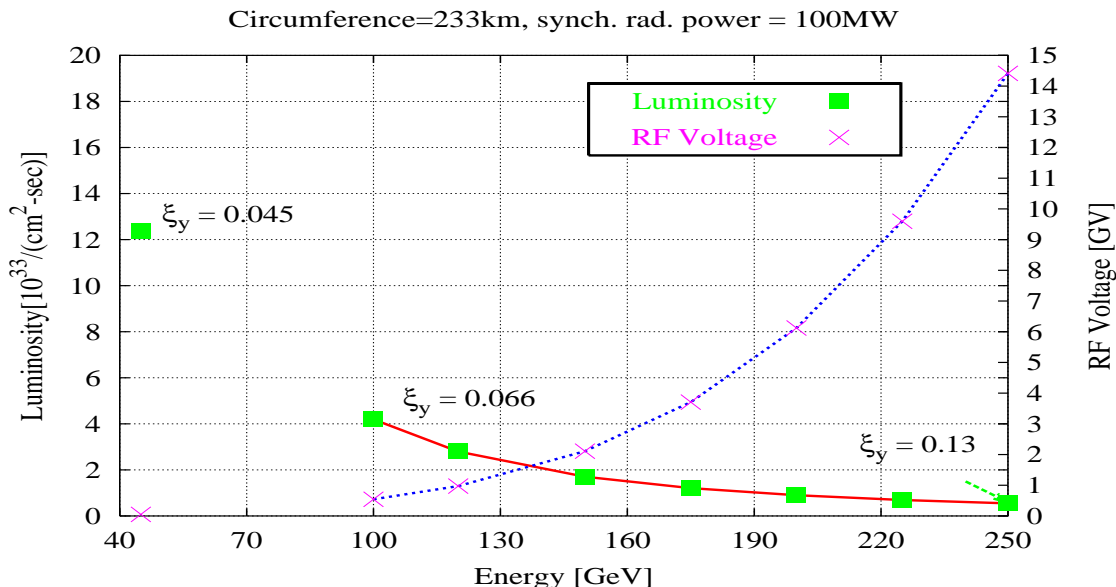


Figure 6: Achievable luminosities and the RF voltages required as a function of energy at a ring circumference of 233km. The synchrotron radiation power is kept constant at 100MW for energies at and above 100 GeV. The beam-beam parameter scales with the damping decrement as discussed in Section 4. The values at 45 GeV are obtained using the design strategy discussed in Section 7.

9 An Injector System

The Fermilab accelerator complex (Linac, Booster and Main Injector) could be used as the basis for an e^+e^- injector if the beam energies were somewhat reduced from those used for protons. The specifications of an injector system could follow the design of the LEP[21] and HERA[25] injectors, or the the APS[26] injection system.

Two new electron linacs would be required. The first would operate at about 3 GHz and accelerate electrons to an energy of around 200 MeV, which would be sufficient to produce positrons. A positron production target would be followed by a second linac section to produce a positron energy high enough to inject into the positron damping ring. Since the positrons will be produced at a much lower flux and larger emittance than electrons, it is necessary to damp and collect positrons from many pulses before further acceleration. The CERN, HERA and APS damping rings are very compact, and operate at energies of around 400 – 600 MeV. The operation of these systems in the same enclosure, parallel to the Fermilab proton linac, seems possible, During the checkout of the FNAL 805 MHz linac upgrade, the linac tunnel was operated essentially with two parallel linacs, so the addition of a e^+e^- linac line would not crowd the existing facility[27].

We have considered the use of the FNAL Booster to accelerate the e^+ and e^- to higher energies, however the use of gradient magnets in the lattice makes this ring somewhat inappropriate for electrons, since this lattice affects the damping partition numbers in undesirable ways. In order to eliminate this problem, a correction package, consisting of a gradient magnet and a quadrupole, should be inserted in the ring to correct the damping partition numbers. The booster has sufficient space to accommodate this package. Similar packages

have been used in the PS at CERN.

It is unclear if it is more efficient to reverse the magnetic field in the accelerator structures or build injection lines so beams could circulate in opposite directions. We assume the fields will not be reversed and injection and extraction systems would have to be added to the booster for e^+e^- operation. The maximum energy that could be reached with the existing rf would be around 3 GeV. Since a new proton source is being considered for a neutrino source and muon collider, which would not fit in the existing booster tunnel, there is also the possibility of designing a compact, separated function magnet lattice to replace the existing booster magnets.

We assume electrons and positrons would be injected into the Main Injector (MI) in opposite directions at an energy of around 3 GeV. This energy would require the MI magnets to operate at a much lower field than would ever be used for protons, however the magnets have been measured at this low field and the field quality seems to be acceptable for electron operation[28]. The maximum energy that could be produced in the main injector is around 12 GeV, due to the limited rf, and the limited space for adding more. The beams would then be extracted in opposite directions into the VLHC booster tunnel for acceleration up to the injection energy of the VLHC ring.

A third synchrotron is probably required, since the 12 GeV electrons from the MI injected into the collider ring, would require the average magnetic field to be about 16 Gauss, which should be compared to the 215 Gauss injection field of LEP. We have studied the properties of an electron ring in the tunnel of a low field VLHC booster in the context of an ep collider[29]. Such a ring could have a maximum energy up to about 80 GeV with a installed RF voltage of 1.09 GV. We assume this rf operates at 352 MHz. If the VLHC booster ring was used only as an injector, an injection energy of around 40 GeV could be accommodated with an rf voltage of about 60 MV.

A recent suggestion by E. Keil[11] of building an injector with a beam energy of 45 GeV has a number of desirable results. A higher energy injector makes injection into the high energy ring easier, and raises the transverse mode coupling instability threshold, permitting more intense bunches. In addition the injector is at an energy where it could be carefully optimized for operation as a “Giga Z” Factory, with many tightly spaced bunches circulating in a comparatively small ring. This permits staging, in that the injector can be producing useful physics while the large ring is under construction. When the facility is complete, there would be the opportunity of using the injector for Z^0 physics while the high ring is used for Higgs, SUSY and top quark physics.

10 Technological Challenges

The primary technical challenges seem to be cooling the vacuum chamber, disposing of the heat produced, and determining how low the field of the collider magnets can be confidently run, since this minimum field determines the design of the magnets and the injection energy. In addition, however, there are a number of other technical problems which must be considered.

10.1 Vacuum System

Besides the usual synchrotron radiation induced gas desorption, the vacuum chamber design is determined by a number of constraints. Although the power density of the synchrotron

radiation deposition is smaller than many other storage rings and synchrotron sources, the critical energy of the synchrotron photons spans a large range, (5 - 500 keV), and the large bend radius complicates the power deposition. In addition the large circumference requires a design which both minimizes beam wall interactions and is inexpensive.

The large range in critical energy of the synchrotron radiation implies that the power in *low* energy beams will be deposited mostly inside the vacuum chamber, but the chamber will become transparent to *high* energy photons, so external absorbers are required for high energies. The high energy photons will also be subject to internal reflection at grazing incidence, but are poorly attenuated by aluminum. These photons are a radiation hazard to electronics and cable insulation, thus the absorbers must be shielded to insure useful radiation levels in the tunnel.

The large bending radius complicates even deposition of synchrotron radiation power on the vacuum chamber walls, since these chambers would be expected to move slightly with operational temperature fluctuations and the motion of the earth. Since deposition on the wall is not expected to be constant, we assume that the vacuum chamber would have an ante-chamber which would conduct the synchrotron radiation to lumped absorber / window assemblies where the power could be absorbed and the synchrotron radiation outgassing could be pumped.

In order to minimize both beam-wall interactions and the cost and complexity of the vacuum system, it may be desirable to use prebaked chambers, and welding the aluminum vacuum sections in-situ, without a subsequent bake out[30]. This makes assembly easier, eliminates the need for bellows with a large mechanical range, reduces the rf loss factor induced by the bellows on the beam (both due to the number and complexity of bellows), and reduces the cost and complexity of the vacuum system as a whole. Since the chamber will heat up somewhat during normal operation, some bellows are required. It is, however, highly desirable to avoid the expansion involved in a high temperature bake, ($\Delta l = \alpha l \Delta T = 2.4 \cdot 10^{-5} 100 100 = 24$ cm), for lengths l and ΔT of 100 m and 100 deg C. In order to do this, one must have sufficient pumping in the chamber to insure that a pressure of 10^{-8} Torr can be achieved, which would allow a beam lifetime of about an hour, and permit subsequent wall scrubbing by synchrotron radiation.

10.2 Cooling System

The warm water produced in the synchrotron absorbers is also a concern. Since there will be roughly 100 MW of heating, distributed over 230 km, we assume this heat must be brought to the surface where cooling towers would be used to discharge it into the atmosphere. This system would be a significant environmental perturbation on the surface. We have also looked at discharging the heat into the ground and into surface water. Since the tolerable thermal range of the system is fairly narrow, due to the fact that thermal expansion must be minimized, the temperature range of the water would also be comparatively limited, thus it would be difficult to recover any useful power from the waste water.

10.3 Magnet Design

The primary issue with the injector system design is determining the minimum field where the ring magnets can usefully transport beam. Since the bending magnets in the arcs operate at a field of $B_{inj}[\text{Gauss}] = 1.3 E[\text{GeV}]$, and the error fields at injection should be below $(10^{-4} - 10^{-3})B_{inj}$, error fields due external sources, other components and remanent

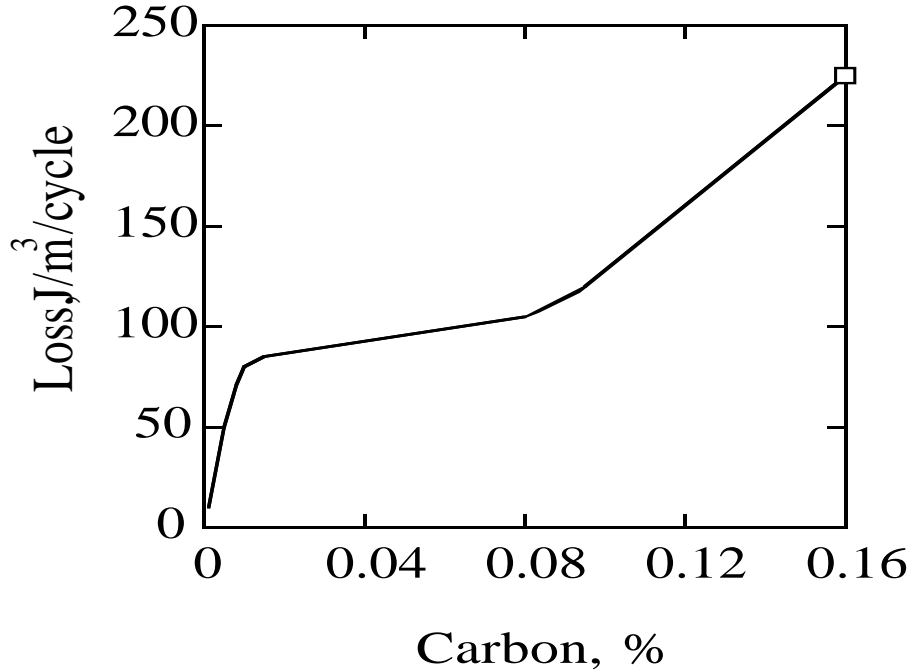


Figure 7: Hysteresis loss as a function of carbon content in steel.

fields, could be a problem. A final injector synchrotron must then be designed which can produce beams in the required energy. This synchrotron can be located in the tunnels which would be eventually occupied by the hadron booster.

We have shown that external fields can be well attenuated by the magnet yoke itself and extensive shielding of magnets may not be required[5] [22]. The remanent fields at low excitation are a function of the specific alloy used, and number of alloys exist with very low remanent fields, however their costs tend to be higher than steel. One option seems to be the use of vacuum or hydrogen annealed steel [23]. This anneal removes carbon from the steel very efficiently, reducing the remanent field and hysteresis losses by a significant factor, as shown in Figure 5 [24]. It seems as though an order of magnitude reduction in remanent fields from the standard low carbon 1010 alloy, ($\sim 0.1\%$ carbon), may be possible, in an alloy which is not significantly more expensive than standard commercially produced ones.

10.4 Other Components

A number of other systems and design issues have not been considered in any significant detail in this paper. We assume that superconducting RF cavities will be necessary. The design of these cavities must suppress higher order modes efficiently.

It is not clear if the $e^+ - e^-$ collider arcs would be optimized with one or two rings. While it is possible to assume that pretzel orbits can be produced in the comparatively long arcs, it is not clear if parasitic collisions will produce significant emittance growth to justify the construction of a second set of arc magnets. This may significantly affect the cost.

The placement of the rf cavities will determine the energy of the beam around the ring. Since so much energy is added per turn, it may be necessary to distribute the cavities around

the ring. This might require zero dispersion straights at a number of locations.

If the $e^+ - e^-$ collider and the low field hadron collider magnets are both energized at the same time, the lepton collider will need to be protected from the fringe fields of the hadron collider. These fringe fields at a distance of about a meter are of the order of a few hundred Gauss, about the same level as the main bending field in the lepton collider.

Extensive masking and collimation systems will be required to protect the detector components from synchrotron radiation.

11 Conclusions

We have explored the feasibility of a large electron-positron collider within the context of a staged approach to building a very large hadron collider. We have shown that in a ring of circumference 233 km, a lepton collider with $200 \leq E_{cm} \leq 500$ GeV with synchrotron radiation power limited to 100 MW would require RF voltages comparable to LEP and would achieve luminosities in the range $0.5 - 4 \times 10^{33} \text{ cm}^{-2}\text{sec}^{-1}$ with conservative choices of beam parameters. The achievable energy extends to nearly 800 GeV (center of mass) at a lower luminosity of $10^{32} \text{ cm}^{-2}\text{sec}^{-1}$ but an unrealistic RF voltage is required to replenish the energy lost by the beam.

Such a machine derives benefits from its size and operating energy, in that the limiting beam-beam tune shifts may be much higher than even those seen at LEP. In addition it may be possible to further optimize the operation of this machine, particularly the interaction regions, to operate with a smaller β^* than was used in LEP. A preliminary IR design [12] shows that $\beta_y^* = 1$ cm may be feasible. There are a number of issues which require more study, in particular methods of working around the limitations imposed by the transverse mode coupling instability. The polarization of the beam which can be achieved also requires better quantification, and there are a number of concepts which we were unable integrate in the design.

We believe that a lepton collider in a tunnel built to house a very large hadron collider is technically feasible. The important question to answer first is whether the physics at these energies is sufficiently interesting. Assuming that is the case, the design of such an accelerator can proceed to the next stage. The cost of the technical components in the lepton collider will likely be dominated by the superconducting RF cavities. Improvements in design and technology can be expected to reduce the cost a decade from now compared to what they are today. Several technical challenges have to be faced but none appear to be insurmountable.

Acknowledgements

We thank Ernie Malamud for initiating this study, and Alvin Tollestrup for his encouragement. We would also like to acknowledge many useful suggestions and comments by Eberhard Keil, Oswald Grobner, Ralph Assmann and Karel Cornelis of CERN, Gerry Dugan and Richard Talman of Cornell, Desmond Barber of DESY, and Lee Teng and Sushil Sharma of Argonne.

References

- [1] Annual VLHC meeting, October 2000, Port Jefferson
- [2] C. Hill, Workshop on an e+e- Storage Ring at the VLHC, IIT, March 9-11, 2001, Chicago, IL, http://capp.iit.edu/capp/workshops/epem/ee_workshop_schedule.html
- [3] Workshop on an e+e- Storage Ring at the VLHC, IIT, March 9-11, 2001, Chicago, IL, http://capp.iit.edu/capp/workshops/epem/ee_workshop.html
- [4] D. Brandt et al., *Accelerator Physics at LEP*, Reports on Progress in Physics, **63**, 939 (2000)
- [5] J. Norem, E. Keil, *A High Energy $e^+ - e^-$ collider in a "Really Large" Tunnel*, ANL-HEP-CP-96-94, 1996
- [6] E. Keil, Workshop on an e+e- Ring at VLHC, Illinois Insitute of Technology, March 2001
- [7] G. Dugan, Workshop on an e+e- Ring at VLHC, Illinois Insitute of Technology, March 2001
- [8] A. Burov, et al., *Beam stability issues in very large hadron collider*, NIM Section A, Vol. 450, pg 194 (2000)
- [9] J. Jowett, Proc. Fourth Workshop on LEP Performance, Chamonix, January 1994 ed. J. Poole, CERN-SL/94-06, pg 47 (1994)
- [10] S. Peggs, Workshop on Synchrotron Radiation Effects in the VLHC, BNL (Sept 2000)
- [11] E. Keil, CERN, personal communication, (2001)
- [12] C. Johnstone, T. Sen, *Lattice Design for a Very Large Lepton Collider*, Proc. of the Workshop on an e+e- Ring at VLHC, Illinois Insitute of Technology, March 2001
- [13] E. Keil, R. Talman, *Part. Acc.*, **14**,p 109 (1983)
- [14] D. Barber, in *Handbook of Accelerator Physics and Engineering*, edited by A. Chao and M Tigner (World Scientific, 1999)
- [15] J. Buon and J.P. Koutchouk, *Polarization of Electron and Proton Beams*, CERN Yellow Report 95-06, Vol II, pg 879 (1995)
- [16] Desmond Barber, DESY, personal communication (April 2001).
- [17] D. Barber et al. *High spin polarization in the HERA electron storage ring*, NIM A, **338**, 166 (1994)
- [18] H. Wiedemann, Nucl. Instr. Methods, **172**, 33 (1980)
- [19] M. Sands, SLAC Report SLAC-121 (1970)
- [20] A. Chao, *Frontiers of Particle Beams*, Lecture Notes in Physics Vol. 296, pg 51 (1988)
- [21] The LEP Injector Study Group, *LEP Design Report: Vol.I, The LEP Injector Chain* CERN-LEP/TH/83-29, 1983.
- [22] J. Norem, J. Jagger, S. Sharma, E. Keil, G. W. Foster, E. Malamud, E. Chojnacki, D. Winn, *An e+e- Top Factory in a 50+t0 TeV Hadron Collider Tunnel*, Proceedings of the 1997 PAC Conference, Vancouver, 363, (1997)
- [23] C. W. Chen, *Magnetism and metallurgy of Soft Magnetic Materials*, North-Holland, Amsterdam, (1977).

- [24] J. R. Davis, ed., *Metals Handbook, Desk Edition, Second Edition*, The Materials Information Society, Materials Park, Oh, (1998)
- [25] G. Stange, IEEE Trans. Nucl Sci. **NS-26** (1979) 4146.
- [26] *Annex to 7-GeV Advanced Photon Source Conceptual Design Report*, Argonne Report ANL-87-15 Annex, (1987).
- [27] R. Noble, Fermilab, personal communication, (1997)
- [28] B. Brown, Fermilab, personal communication, (1997)
- [29] M. Derrick, H. Friedsam, A. Gorski, S. Hanuska, J. Jagger, D. Krakauer, J. Norem, E. Rotela, S. Sharma, L. Teng, K. Thompson, T. Sen, E. Chojnacki, D. P. Barber, *An ep Collider with $E_{cm} = 1$ TeV in a VLHC Tunnel*, Proceedings fo the 1999 Particle Accelerator Conference, New York (1999) 2635
- [30] O. Grobner, CERN, personal communication, (2001)
- [31] R. Kleiss and H. Burkhardt, Computer Physics Communications, **81**, 372 (1994)
- [32] H. Burkhardt, Proceedings of the 3rd Workshop on LEP performance (Chamonix), J. Poole (ed.), CERN SL/93-19

A Appendix: Useful Symbols and Formulae

c	Velocity of light
e	Electron charge
E	Beam energy
f_{rev}	Revolution frequency
h	Harmonic number
\mathcal{H}	Lattice factor = $[\eta^2 + (\beta\eta' - \beta'\eta/2)^2]/\beta$
I_b	Bunch current
I	Beam current in a single beam
J_x, J_y, J_s	Horizontal and Longitudinal partition numbers
k_{\perp}, k_{\parallel}	Transverse, Longitudinal loss factor
\mathcal{L}	Luminosity
m_e	Electron mass
M_b	Number of bunches in the ring
N_b	Number of particles in a bunch
P_T	Synchrotron power lost in both beams
r_e	Classical electron radius
R	Arc radius
V_{RF}	Maximum RF voltage
α_c	momentum compaction
β_x, β_y	Beta function at some point in the ring
β_x^*, β_y^*	Beta function at at the interaction point
γ	Relativistic factor
δ	Momentum variation
ϵ_x, ϵ_x	Horizontal, Vertical emittance
η	Slip factor
κ	Emittance ratio = ϵ_y/ϵ_x
λ_d	Damping decrement
μ_x, μ_y	Phase advance per cell
ν_s	Synchrotron frequency
ν_x, ν_y	Arc tunes
ξ_x, ξ_y	Beam beam tune shift
ρ	Bending radius
σ_x, σ_y	Beam radius
σ_E	Bunch energy spread
σ_x^*, σ_x^*	Beam radius at interaction point
τ_L	Beam lifetime
ϕ_s	Synchrotron phase

Luminosity

$$\mathcal{L} = \frac{N_{e^+} N_{e^-} M_b f_{rev}}{4\pi} \frac{1}{\sqrt{\beta_{x,e}^* \epsilon_{x,e} \sqrt{\beta_{y,e}^* \epsilon_{y,e}}}} \quad (\text{A.1})$$

where N_{e^+} , N_{e^-} are the bunch intensities, M_b is the number of bunches.

Equilibrium horizontal emittance

$$\epsilon_x = \frac{C_q \gamma^2}{J_x} \left[\frac{\oint \mathcal{H} / \rho^3 ds}{\oint 1 / \rho^2 ds} \right] \quad (\text{A.2})$$

The equilibrium emittance in a lattice built entirely with FODO cells scales with the horizontal phase advance μ_x^C per FODO cell as [18]

$$\epsilon_x(\mu_x^C) = 4 \frac{C_q \gamma^2}{J_x} \theta^3 \frac{1 - \frac{3}{4} \sin^2(\mu_x^C/2) + \frac{1}{60} \sin^4(\mu_x^C/2)}{\sin^2(\mu_x^C/2) \sin \mu_x^C}. \quad (\text{A.3})$$

where $C_q = (55/32\sqrt{3})\hbar/mc = 3.84 \times 10^{-13} \text{m}$, J_x is the horizontal damping partition number and θ is the bending angle in half of the FODO cell.

Momentum compaction

$$\alpha_C \approx \frac{L_{Arc}}{C} \frac{\theta^2}{\sin^2(\mu_c/2)} \quad (\text{A.4})$$

where L_{Arc} , C are the lengths of the arcs and the circumference respectively, θ is the bend angle per half cell and μ_c is the phase advance per cell.

Equilibrium energy spread

$$\frac{\sigma_E}{E} \simeq \sqrt{\frac{C_q}{J_s \rho}} \gamma \quad (\text{A.5})$$

where

$$C_q = \frac{55}{32\sqrt{3}} \frac{\hbar c}{mc^2} = 3.84 \times 10^{-13} \text{m}$$

for electrons and positrons. J_s is the longitudinal damping partition number, ρ is the bending radius.

Equilibrium bunch length

$$\sigma_l = \frac{c |\eta| \sigma_E}{\omega_s E} = \frac{c}{\sqrt{2\pi} f_{rev}} \sqrt{\frac{|\eta| E}{h e V_{RF} \cos \psi_s} \frac{\sigma_E}{E}} \quad (\text{A.6})$$

where η is the slip factor, ω_s is the angular synchrotron frequency and the other symbols have their usual meanings.

Energy acceptance

$$\left(\frac{\Delta E}{E} \right)_{accept} = \sqrt{\frac{e V_{RF}}{\pi h |\eta| E} G(\phi_s)} \quad (\text{A.7})$$

$$G(\phi_s) = 2 \cos \phi_s - (\pi - 2\phi_s) \sin \phi_s$$

Beam-beam tune shifts

$$\xi_x = \frac{N_e r_e \beta_x^*}{2\pi \gamma \sigma_x^* (\sigma_x^* + \sigma_y^*)}, \quad \xi_y = \frac{N_e r_e \beta_y^*}{2\pi \gamma \sigma_y^* (\sigma_x^* + \sigma_y^*)} \quad (\text{A.8})$$

In the limit $\sigma_x^* \gg \sigma_y^*$,

$$\xi_x = \frac{N_e r_e \beta_x^*}{2\pi\gamma(\sigma_x^*)^2}, \quad \xi_y = \frac{N_e r_e \beta_y^*}{2\pi\gamma\sigma_x^* \sigma_y^*} \quad (\text{A.9})$$

Energy lost by electrons per turn

$$U = C_\gamma \frac{E^4}{\rho}, \quad C_\gamma = \frac{4\pi}{3} \frac{r_e}{(m_e c^2)^3} = 8.86 \times 10^{-5} \text{m/GeV}^3 \quad (\text{A.10})$$

Synchrotron radiation power in beam

$$P_{synch} = \frac{U I_e}{e} \quad (\text{A.11})$$

Critical energy

$$E_{crit}[\text{keV}] = 2.218 \frac{E^3}{\rho}, \quad E \text{ in GeV}, \rho \text{ in m} \quad (\text{A.12})$$

Critical Wavelength

$$\lambda_{crit} = \frac{4\pi\rho}{3\gamma^3} \times 10^{10}, \quad \text{in Angstroms} \quad (\text{A.13})$$

Number of photons emitted per second by a particle

$$N_\gamma = \frac{15.0\sqrt{3}}{8.0} \frac{P_{synch}}{e N_e E_{crit}} \times 10^3 \quad (\text{A.14})$$

where P_{synch} is in MW, E_{crit} is in keV.

Total Photon Flux

$$\dot{N}_\gamma = 8.08 \times 10^{17} \times I[\text{mA}]E[\text{GeV}], \quad \text{photons/sec} \quad (\text{A.15})$$

Gas Load

$$Q_\gamma = 4.5 \times 10^{-20} \eta_{photo} \phi_\gamma, \quad [\text{Torr} - \text{litres/m/sec}] \quad (\text{A.16})$$

where η_{photo} is the photo-desorption coefficient and $\phi_\gamma = \dot{N}_\gamma / L_{Arc}$ is the photon flux per unit length.

Damping partition numbers

$$J_s \simeq 2.0 \quad (\text{A.17})$$

$$J_x + J_y + J_s = 4 \quad (\text{A.18})$$

For a FODO cell in the thin-lens approximation

$$\frac{dJ_x}{d\delta} = -4 \frac{L_D}{L_Q} \left[\frac{2 + \frac{1}{2} \sin^2 \mu/2}{\sin^2 \mu/2} \right] \quad (\text{A.19})$$

Damping times

$$\tau_0 = \frac{E}{f_{rev} U}, \quad \tau_s = \frac{2}{2 + \mathcal{D}} \tau_0 \approx \tau_0, \quad \tau_y = 2\tau_0, \quad \tau_x = \frac{2}{1 - \mathcal{D}} \tau_0 \approx \tau_y \quad (\text{A.20})$$

$$\mathcal{D} = \frac{\langle \frac{D}{\rho^2} (\frac{1}{\rho} + 2 \frac{B'}{B}) \rangle}{\langle \frac{1}{\rho^2} \rangle} \quad (\text{A.21})$$

Longitudinal quantum lifetime

$$\tau_{quant;s} = \frac{\tau_s}{N_{QL}^2} \exp\left[\frac{1}{2}N_{QL}^2\right] \quad (\text{A.22})$$

where

$$N_{QL} = \left(\frac{\Delta E_{RF}}{\sigma_E}\right)$$

ΔE_{RF} is the energy acceptance of the bucket provided by the RF system, σ_E is the sigma of the energy distribution and τ_s is the longitudinal synchrotron radiation damping time. This is the expression due to Sands [19] but there are other (perhaps more accurate) expressions. **Transverse quantum lifetime**

$$\tau_{quant;\beta} = \frac{e^{r_\beta}}{2r_\beta} \tau_\perp \quad (\text{A.23})$$

where

$$r_\beta = \frac{1}{2} \left(\frac{x_{Apert,\beta}}{\sigma_\beta}\right)^2$$

$x_{Apert,\beta}$ is the transverse position of the aperture limitation, σ_β is the transverse sigma of the particle distribution and $t_{damp,\perp}$ is transverse synchrotron radiation damping time. If there is finite dispersion at the location of the aperture limitation, then Chao's formula [20] holds

$$\tau_{quant;\beta} = \frac{1}{\sqrt{2\pi}} \frac{\exp[r_{\beta,\delta}]}{(2r_{\beta,\delta})^{3/2}} \frac{1}{(1+f)\sqrt{f(1-f)}} \tau_\perp \quad (\text{A.24})$$

where

$$r_{\beta,\delta} = \frac{1}{2} \left(\frac{x_{Apert,\beta}}{\sigma_T}\right)^2, \quad \sigma_T^2 = \sigma_x^2 + D_x^2 \sigma_\delta^2, \quad f = \frac{D_x^2 \sigma_\delta^2}{\sigma_T^2}$$

D_x is the dispersion at the location of the aperture, σ_δ is the relative momentum deviation. For a fixed transverse damping time, the quantum lifetime depends on the parameters $f, r_{\beta,\delta}$ and has minimas at specific values of these parameters.

e^+e^- Bremsstrahlung cross-section

The dominant process which determines the lifetime at collision is small angle forward radiative Bhabha scattering which has a cross-section given by [32]

$$\sigma_{e^+e^-} = \frac{16}{3} \alpha r_e^2 \left[-\left(\ln\left(\frac{\Delta E}{E}\right)_{accept} + \frac{5}{8}\right) \left(\ln(4\gamma_{e^+}\gamma_{e^-}) - \frac{1}{2}\right) + \frac{1}{2} \ln^2\left(\frac{\Delta E}{E}\right)_{accept} - \frac{\pi^2}{6} - \frac{3}{8} \right] \quad (\text{A.25})$$

where $(\Delta E/E)_{accept}$ is the RF acceptance of the bucket.